JOURNAL OF GUIDANCE, CONTROL, AND DYNAMICS
Vol. 30, No. 5, September–October 2007

Convex Programming Approach to Powered Descent Guidance for Mars Landing

Behçet Açıkmeşe* and Scott R. Ploen†
Jet Propulsion Laboratory, California Institute of Technology, Pasadena, California 91109

DOI: 10.2514/1.27553

We present a convex programming algorithm for the numerical solution of the minimum fuel powered descent guidance problem associated with Mars pinpoint landing. Our main contribution is the formulation of the trajectory optimization problem, which has nonconvex control constraints, as a finite-dimensional convex optimization problem, specifically as a second-order cone programming problem. Second-order cone programming is a subclass of convex programming, and there are efficient second-order cone programming solvers with deterministic convergence properties. Consequently, the resulting guidance algorithm can potentially be implemented onboard a spacecraft for real-time applications.

Nomenclature

A, B	=	matrices describing the discrete time dynamics
$f(\cdot)$	=	the function f: IR $\rightarrow$ IR^n over a time interval $[0, t_f]$
g	=	gravitational acceleration vector of Mars
g_e	=	magnitude of Earth's gravity
H	=	Hamiltonian of the system
I	=	identity matrix of appropriate dimensions
I_{sp}	=	specific impulse for thrusters
IR	=	the set of real numbers
IR^n	=	the space of n-dimensional real vectors
m	=	spacecraft mass
m_{wet}	=	spacecraft initial mass with the fuel
$\hat{n}_f$	=	final thrust direction
$\hat{n}_0$	=	initial thrust direction
p_k	=	vector coefficients for basis function ϕ_k
$Q = Q^T > 0$	=	denotes that the symmetric matrix Q is positive definite
R_0, R_1, R_2	=	functions defining the Hamiltonian
r	=	surface relative spacecraft position vector
r_0	=	spacecraft initial position vector
$\dot{r}$	=	surface relative spacecraft velocity vector
$\dot{r}_0$	=	spacecraft initial velocity vector
S_j, v_j, a_j	=	matrices, vectors, and scalars defining the convex state constraints
T_c	=	net thrust force vector acting on the spacecraft
T_1 and T_2	=	lower and upper bounds on the available thrust for the thrusters
t_f	=	time of flight for powered descent
t_f^*	=	optimal time of flight
u	=	net control acceleration induced by the thrusters
v	=	unit vector describing a thrust pointing constraint
x	=	augmented spacecraft position and velocity vector
z	=	natural logarithm of mass
α	=	constant describing mass consumption rate
Γ	=	slack variable that bounds thrust magnitude
η	=	augmented vector of p_k, $k = 1, \ldots, M$
θ_{alt}	=	glide slope angle
$\tilde{\theta}_{\text{alt}}$	=	bound on the allowable glide slope angle
λ	=	costate vector
ρ_1	=	lower bound on thrust magnitude
ρ_2	=	upper bound on thrust magnitude
σ	=	mass normalized slack variable
$\Phi_k, \Lambda_k, \Psi_k, \Upsilon_k$	=	matrices describing the state transition in discrete time
ϕ	=	cant angle for the thrusters
ϕ_k	=	basis functions for numerical discretization
$\|x\|$	=	2-norm of vector x, $\sqrt{x^T x}$

I. Introduction

IN THIS paper we present a convex programming algorithm for the powered descent guidance problem for Mars pinpoint landing. This problem is motivated by future pinpoint landing missions that are gaining importance due to the renewed interest in the manned and robotic exploration of Mars. The pinpoint landing problem can be defined as guiding a lander spacecraft to a given target on the planet's surface with an accuracy of fewer than several hundred meters. As a result, the solution algorithm can also be used to solve the powered descent guidance problems for the moon and other planetary pinpoint landing missions.

To ensure a safe landing on Mars, landing sites for first-generation Mars missions such as Viking and Mars Pathfinder were determined by considering the scientific merit of various sites as well as the overall terrain quality (e.g., slope, roughness). Because these missions were exploratory in nature, the exact location of the landing site within the error ellipse was not critical. For example, landing accuracy was approximately 150 km for Mars Pathfinder and 35 km for the Mars Exploration Rovers. The Mars Surface Laboratory mission scheduled for launch in 2009 will further increase landing accuracy resulting in a delivery of the lander to within 10 km.

In next generation Mars missions the need to perform pinpoint landing will be required. Further improvements in landing accuracy require enhancements to heritage flight systems and are discussed in detail in [1]. For example, it may be required to land next to scientifically interesting targets located within hazardous terrain, or

Presented as Paper 6288 at the AIAA Guidance, Navigation, and Control Conference and Exhibit, San Francisco, 15–18 August 2005; received 28 August 2006; accepted for publication 2 January 2007.

*Senior Engineer, Guidance and Control Analysis Group, Mail Stop 198-326; Behcet.Acikmese@jpl.nasa.gov. Member AIAA (Corresponding Author).

†Senior Engineer, Guidance and Control Analysis Group, Mail Stop 198-326; Scott.R.Ploen@jpl.nasa.gov. Member AIAA.

to land in close proximity to other prepositioned surface assets such as a rover from a previous mission. Further, human missions will require the crew to land near prepositioned cargo or fuel.

Mars pinpoint landing involves an entry phase through the Mars atmosphere, a phase of descent with a parachute, and then the final phase of *powered descent*, which is initiated with the parachute cutoff. The powered descent guidance problem for pinpoint landing is defined as finding the fuel optimal trajectory that takes a lander with a given initial state (position and velocity) to a prescribed final state in a uniform gravity field, with magnitude constraints on the available net thrust, and various state constraints. A version of this problem is also known in the optimal control literature as the *soft-landing problem* [2], and its solutions have well-known characterizations ([3] pp. 28–33). One important characterization is that the net thrust magnitude must be either at the minimum or maximum value at any given time during the maneuver. A closed-form solution of the problem for the 1-D case (with vertical motion only) is given by [2,4]. However, to the best of our knowledge, a closed-form solution of the optimal thrust profile is not available for the general 3-D case with additional state and control constraints. A trajectory based on a quartic polynomial in time was used during the Apollo mission [5]. Various other approaches to obtain both numerical and approximate solutions of the pinpoint landing terminal guidance problem have been described over the last few years. More recently, in [6] the first-order necessary conditions for the problem are developed, and it is shown that the optimal thrust profile has a maximum-minimum-maximum structure. Numerical solutions are obtained for various initial conditions by converting the guidance problem into a constrained nonconvex parameter optimization problem using both direct collocation and direct multiple shooting methods. In [7] Legendre pseudospectral methods are used to develop a numerical solution to the pinpoint landing guidance problem. In [8] an approximate analytical solution is developed by solving a related optimal control problem that does not use a minimum fuel cost functional.

Direct numerical methods for trajectory optimization are attractive because explicit consideration of the necessary conditions (adjoint equations, transversality conditions, maximum principle) are not required [9]. The infinite-dimensional optimal control problem is directly converted into a finite-dimensional parameter optimization problem [10–12], which is then solved via a nonlinear programming method. However, a real-time onboard solution of a nonlinear program via a general iterative algorithm may not be desirable without explicit knowledge of the convergence properties of the algorithm. Because Mars pinpoint landing requires real-time onboard computation of the optimal trajectory, it is essential to exploit the structure of the problem to design algorithms with guaranteed convergence to the global optimum with a deterministic convergence criteria. This leads us to formulate the problem in a convex optimization [13,14] framework. Specifically, we formulate the resulting parameter optimization problem as a second-order cone programming problem (SOCP) that is a subclass of convex programming [15]. SOCP problems have low complexity, and they can be solved in polynomial time. There exist algorithms, such as interior-point methods [16–18], that compute an optimal solution[‡] with a deterministic stopping criteria, and with prescribed level of accuracy. This implies that the global optimum can be computed to any given accuracy with a deterministic upper bound on the number of iterations needed for the convergence of the iterative algorithm. Therefore, numerical SOCP solution algorithms are very promising for real-time onboard computations.

We first formulate the powered descent guidance problem for the pinpoint landing as a fuel optimal trajectory optimization problem with state and control constraints. The primary nonconvex constraint in the resulting optimal control problem is on the thrust magnitude. The thrusters cannot be turned off once they are initiated during the maneuver. Further, there are minimum thrust levels below which the thrusters can not operate reliably. Because the spacecraft is modeled as a point mass with a single thruster, there is a lower nonzero bound on the thrust magnitude that defines a nonconvex feasible region in the control space. We introduce a slack variable to relax this nonconvex constraint. Next, it is shown that any optimal solution for the resulting relaxed problem is also optimal for the original problem. Then we approximate the relaxed optimal control problem as a finite-dimensional parameter optimization problem via representing the control input by a finite set of basis functions, which leads to a finite-dimensional convex parameter optimization problem; more specifically it leads to a SOCP. Additionally, we consider thruster pointing constraints and extend our convex solution approach to handle this constraint via a heuristic. Finally, we present some simulation results for an example spacecraft.

Our guidance algorithm involves solution of a SOCP, which has a global optimal solution that can be computed very efficiently by readily available primal-dual interior-point method algorithms with guaranteed convergence to the optimal solution [17,19]. The primal-dual interior-point algorithms are also robust in the sense that, for any given neighborhood of the optimal solution, there exists a finite bound on the number of iterations required for convergence of the algorithm. Consequently, the resulting guidance algorithm can potentially be implemented onboard. This is the major motivation for the proposed approach because the guidance algorithm must be executed autonomously onboard the spacecraft. Note that a generic nonlinear programming algorithm is not appropriate for onboard use because, in general, there exists no guarantee on the convergence to an optimal or even to a feasible solution in a predetermined number of iterations. It is also shown in [20] that the size of the region of feasible initial states, for which there exist feasible trajectories, can be increased drastically (more than twice) with this approach relative to the traditional polynomial-based guidance approaches mentioned earlier. However, one has to be careful about the size of the resulting SOCP problem. Depending on the basis functions used to approximate the control inputs and the discretization of the time, the size of the resulting SOCP can vary significantly. This increases the cost of the computations for each iteration, which is a concern despite the fact that there is a known upper bound on the number of iterations needed for a desired level of convergence to the optimal solution. One way to mitigate this problem is using basis functions that can approximate an optimal control profile with fewer number of functions such as Chebyshev polynomials. Furthermore, future work is needed to further improve the efficiency of the computations by implementing a SOCP solution algorithm specifically tailored for this problem.

The paper is organized as follows: Sec. II presents the continuous-time optimal control problem for Mars pinpoint landing with the control and state constraints, Sec. III presents the main technical result for the convexification of this problem and the resulting relaxed problem (whose optimal solution is also feasible for the original problem), Sec. IV presents the discretization of the continuous-time problem and the resulting finite-dimensional parameter optimization problem, Sec. V presents some simulation results with the thruster magnitude and the state constraints, Sec. VI describes a heuristic to expand the convex solution approach to handle the thruster pointing constraints, and Sec. VII summarizes the conclusions of this paper.

II. Problem Formulation

In this section, we describe the trajectory optimization problem for a generic spacecraft performing pinpoint landing on a planet with uniform gravitational field. This problem description also includes Mars powered descent guidance. Because the powered descent phase of a landing mission starts at a low altitude relative to planet's radius (this altitude is less than 5 km for Mars landing), the uniform gravity assumption is appropriate. Other forces such as aerodynamic forces due to winds are neglected in optimal trajectory design and they will be treated as disturbances. The aerodynamic forces are dominant in the atmospheric entry, where velocities are in the order of several thousands of meters per second, and the parachute phases of the mission. At the start of the powered descent phase, the parachute is

[‡]Throughout the paper, optimal solution of an optimal control or a parameter optimization problem will always refer to a *global* optimal solution of the problem.

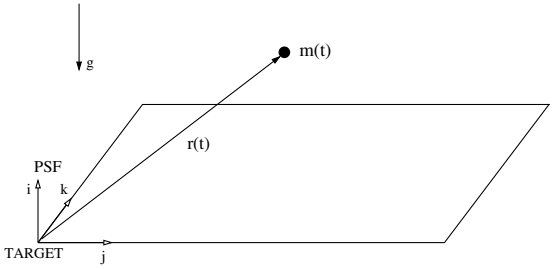

Fig. 1 Surface fixed coordinate frame.

already released and the velocity is typically on the order of a hundred meters per second. Consequently, the accelerations due to aerodynamic forces are much lower than the gravitational accelerations during the powered descent phase of the mission. Also, we do not explicitly consider coupled translational and attitude guidance, which is a significantly more complex problem. As a result, the aforementioned assumptions lead to a problem formulation that involves an optimal control problem with a fuel cost, the spacecraft translational dynamics, and various state and control constraints.

Remark 1: There are recent results on the solution of the constrained attitude guidance problem in a semidefinite programming (SDP) framework [21,22], which can potentially lead to a solution of the coupled translation and attitude powered descent guidance problem. □

The translation dynamics of the spacecraft are expressed in a *surface fixed* frame of reference (PSF), Fig. 1, as

$$\ddot{r}(t) = g + \frac{T_c(t)}{m(t)} \tag{1}$$

$$\dot{m}(t) = -\alpha \|T_c(t)\| \tag{2}$$

where $r \in \mathrm{IR}^3$ is the position vector relative to the target, $g \in \mathrm{IR}^3$ is the constant gravitational acceleration vector of the planet, $T_c \in \mathrm{IR}^3$ is the net thrust vector, m is the spacecraft mass, and α is a positive constant describing the fuel consumption rate. We assume that there are n identical thrusters with equal thrust levels T at each time with a specific impulse given by I_{sp}. Then,

$$T_c = (nT\cos\phi)e \quad \text{and} \quad \alpha = \frac{1}{I_{\mathrm{sp}} g_e \cos\phi}$$

where $g_e = 9.807\ \mathrm{m/s^2}$ is the Earth's gravitational constant, $e \in \mathrm{IR}^3$ is a unit vector describing the instantaneous thrust direction, and ϕ is the cant angle of the thrusters to e (net thrust direction, see Fig. 2). Thrust for each thruster T is bounded as

$$0 < T_1 \le T(t) \le T_2$$

for all time during the descent. This implies that

$$\rho_1 \le \|T_c(t)\| \le \rho_2, \quad \forall\ t \in [0, t_f] \tag{3}$$

where $\rho_2 > \rho_1 > 0$ are given by

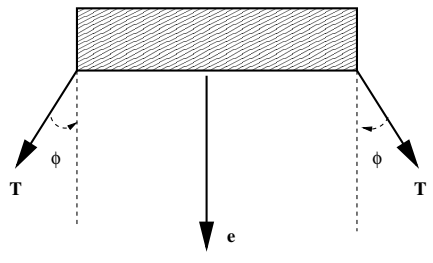

Net thrust direction

Fig. 2 Spacecraft geometry.

$$\rho_1 = nT_1\cos\phi, \qquad \rho_2 = nT_2\cos\phi$$

and t_f is the final time for the powered descent landing. Note that the constraint (3) describes a nonconvex region in the control space. The initial and final position and velocity, and the initial mass are specified,

$$m(0) = m_{\mathrm{wet}}, \qquad r(0) = r_0, \qquad \dot{r}(0) = \dot{r}_0 \tag{4}$$

$$r(t_f) = 0, \qquad \dot{r}(t_f) = 0 \tag{5}$$

where r_0, $\dot{r}_0$ are constant vectors, and m_{wet} is the initial mass of the landing vehicle. In the rest of the paper, we assume that

$$r_{0_1} > 0 \tag{6}$$

where r_{0_1} is the component of the initial position vector along the direction opposite to the direction of the gravity. Also, it is required that the trajectory does not go below the surface during the maneuver, that is,

$$r_1(t) \ge 0, \quad \forall\ t \in [0, t_f] \tag{7}$$

where $r(t) = [r_1(t), r_2(t), r_3(t)]^T$. There can be additional state constraints in terms of the position or the velocity (e.g., to avoid obstacles). It is assumed that these state constraints have the following general form:

$$\|S_j x(t) - v_j\| + c_j^T x(t) + a_j \le 0, \qquad j = 1, \ldots, n_s, \quad \forall\ t \in [0, t_f] \tag{8}$$

where $S_j \in \mathrm{IR}^{n_j \times 6}$, $c_j \in \mathrm{IR}^6$ with $n_j \le 6$, $v_j \in \mathrm{IR}^{n_j}$, $a_j \in \mathrm{IR}$, and $x \in \mathrm{IR}^6$ is the part of the state vector corresponding to position and velocity defined by

$$x = \begin{bmatrix} r \\ \dot{r} \end{bmatrix} \tag{9}$$

Clearly constraint defined by inequality (7) can be considered under the class of constraints defined by inequality (8). A bound on the velocity, $\hat{V}$, can be imposed by

$$\|\dot{r}(t)\| \le \hat{V} \quad \text{for } t \in [0, t_f] \tag{10}$$

Another state constraint is "altitude angle" or "glide slope" constraint that can be defined by the lateral and vertical position of the spacecraft relative to the target as

$$\theta_{\mathrm{alt}}(t) \triangleq \arctan\left\{\frac{\sqrt{r_2(t)^2 + r_3(t)^2}}{r_1(t)}\right\}$$

To impose $\theta_{\mathrm{alt}}(t) \le \tilde{\theta}_{\mathrm{alt}} \le \frac{\pi}{2}$ for all $t \ge 0$, the following form of (8) is used:

$$\|Sx\| + c^T x \le 0 \tag{11}$$

where

$$S = \begin{bmatrix} 0 & 1 & 0 & 0 & 0 & 0 \\ 0 & 0 & 1 & 0 & 0 & 0 \end{bmatrix}, \qquad c = \begin{bmatrix} -\tan\tilde{\theta}_{\mathrm{alt}} & 0 & 0 & 0 & 0 & 0 \end{bmatrix}^T$$

Given the state and control constraints, the minimum fuel powered descent trajectory optimization problem associated with the pinpoint landing is described as follows:

Problem 1:

$$\max_{t_f, T_c(\cdot)} m(t_f) = \min_{t_f, T_c(\cdot)} \int_0^{t_f} \|T_c(t)\| \, \mathrm{d}t$$

$$\text{subject to } \ddot{r}(t) = g + T_c(t)/m(t), \qquad \dot{m}(t) = -\alpha \|T_c(t)\|$$

$$0 < \rho_1 \le \|T_c(t)\| \le \rho_2, \qquad r_1(t) \ge 0$$

$$\|S_j x(t) - v_j\| + c_j^T x(t) + a_j \le 0, \qquad j = 1, \ldots, n_s$$

$$m(0) = m_{\text{wet}}, \qquad r(0) = r_0, \qquad \dot{r}(0) = \dot{r}_0$$

$$r(t_f) = \dot{r}(t_f) = 0$$

where α, ρ_1, ρ_2, S_j, a_j, c_j, r_0, $\dot{r}_0$ are constant parameters defined in (1–5) and (8). □

Remark 2: In Problem 1, inequality (3) defines nonconvex constraints on the control input. □

Remark 3: Thrust direction can also be constrained at the start and at the end of a maneuver as

$$T_c(0) = \|T_c(0)\| \hat{n}_0, \qquad T_c(t_f) = \|T_c(t_f)\| \hat{n}_f \tag{12}$$

where $\hat{n}_0$ and $\hat{n}_f$ are unit vectors describing the desired thrust directions. □

III. Convexification of the Control Magnitude Constraint

In this section, we first introduce the following modified version of Problem 1:

Problem 2:

$$\min_{t_f, T_c(\cdot), \Gamma(\cdot)} \int_0^{t_f} \Gamma(t) \, \mathrm{d}t \qquad \text{subject to } \dot{m}(t) = -\alpha \Gamma(t) \tag{13}$$

$$\|T_c(t)\| \le \Gamma(t) \tag{14}$$

$$0 < \rho_1 \le \Gamma(t) \le \rho_2 \tag{15}$$

$$\ddot{r}(t) = g + T_c(t)/m(t), \qquad r_1(t) \ge 0$$

$$\|S_j x(t) - v_j\| + c_j^T x(t) + a_j \le 0, \qquad j = 1, \ldots, n_s$$

$$m(0) = m_{\text{wet}}, \qquad r(0) = r_0, \qquad \dot{r}(0) = \dot{r}_0$$

$$r(t_f) = \dot{r}(t_f) = 0$$

where α, ρ_1, ρ_2, S_j, a_j, c_j, r_0, $\dot{r}_0$ are constant parameters defined in (1–5) and (8). □

Problem 2 is obtained by introducing a slack variable Γ to Problem 1. Γ replaces $\|T_c\|$ in the cost and in Eq. (2) and inequality (3) in Problem 1, and it introduces an additional constraint $\|T_c\| \le \Gamma$. Because Problem 2 is merely a relaxation of Problem 1, a solution of Problem 1 clearly defines a feasible solution of Problem 2. However a feasible solution of Problem 2 does not necessarily define a feasible solution of Problem 1. Here we introduce the main technical result of this paper in Lemma 1 that states that the optimal solution of the relaxed problem is also an optimal solution of Problem 1. This leads to a convex solution approach to a nonconvex trajectory optimization problem given by Problem 1, which is obtained by solving Problem 2.

Lemma 1: Consider a solution of Problem 2 given by $[t_f^*, T_c^*(\cdot), \Gamma^*(\cdot)]$. Then, $[t_f^*, T_c^*(\cdot)]$ is also a solution of Problem 1 and $\|T_c^*(t)\| = \rho_1$ or $\|T_c^*(t)\| = \rho_2$ for $t \in [0, t_f^*]$.

Proof: The Hamiltonian for Problem 2 is given by [23,24]

$$H(x, m, T_c, \Gamma, \lambda_0, \lambda) = \lambda_0 \Gamma + \lambda_1^T x_2 + \frac{\lambda_2^T T_c}{m} + \lambda_2^T g - \alpha \lambda_3 \Gamma \tag{16}$$

where $x = [x_1^T, x_2^T]^T$ is the part of the state vector with the position and the velocity, $\lambda_0 \le 0$, $\lambda = [\lambda_1, \lambda_2, \lambda_3]^T \in \mathrm{IR}^7$ is the costate vector. We first state a general form of necessary conditions of optimality given in p. 186 of [23] (Pontryagin's maximum principle). To do that define the state vector $y = [x^T, m]^T \in \mathrm{IR}^7$ and a vector $v = [T_c^T, \Gamma]^T$. Since the set defined by control constraints, Ψ, is a fixed set, any optimal solution defined by the pair $[y^{*T}, v^{*T}]^T$ on $[0, t_f^*]$ must satisfy the following: There exist $\lambda_0 \le 0$ and an absolutely continuous vector function λ such that

1) $[\lambda_0, \lambda(t)^T]^T \ne 0 \ \forall \ t \in [0, t_f^*]$ and

$$\dot{\lambda} = \frac{\partial H}{\partial y}(y^*, v^*, \lambda_0, \lambda) \tag{17}$$

2) *Pointwise maximum principle* given below must be satisfied[§]

$$H(y^*(t), v^*(t), \lambda_0, \lambda) \ge H(y^*(t), v, \lambda_0, \lambda) \quad \forall \ v \in \Psi \quad \text{a.e. on } t \in [0, t_f^*] \tag{18}$$

3) The following *transversality condition* must be satisfied: Let $\psi \triangleq [y^{*T}, v^{*T}, \lambda_0, \lambda^T]^T$, then the vector $[H(\psi(0)), -\lambda(0)^T, -H(\psi(t_f^*)), \lambda(t_f^*)^T]^T$ must be orthogonal to the vector $[0, y^*(0)^T, t_f^*, y^*(t_f^*)^T]$.

The first necessary condition (17) implies that

$$\dot{\lambda}_1 = 0 \tag{19}$$

$$\dot{\lambda}_2 = -\lambda_1 \tag{20}$$

$$\dot{\lambda}_3 = \frac{1}{m^2} \lambda_2^T T_c^*$$

Note that the transversality condition with the given end conditions on the position and velocity vectors at $t = 0$ and $t = t_f^*$ of this problem imply that

$$\lambda_3\left(t_f^*\right) = 0, \qquad H\left(\psi\left(t_f^*\right)\right) = 0$$

Now we show by contradiction that $\lambda_2(t) = 0, \ \forall \ t \in [0, t_f^*]$ is not possible. Since λ_1 is constant and $\lambda_3(t_f^*) = 0$, if $\lambda_2 = 0$, then $\lambda_1 = 0$, as well as $\lambda_3 = 0$. Since $H(\psi(t_f^*)) = 0$, this implies that $\lambda_0 = 0$. This violates the first necessary condition for optimality because it leads to $[\lambda_0, \lambda(t)^T]^T = 0, \ \forall \ t \in [0, t_f^*]$. Consequently, $\lambda_2(t) = 0$ for all $t \in [0, t_f^*]$ does not hold. This implies $\lambda_2(t) = -\lambda_1 t + a$ for some constant a. Since λ_2 is not identically zero, it can be zero at most at one point on $[0, t_f^*]$. We can express the Hamiltonian as

$$H(x(t), m(t), T_c, \Gamma, \lambda_0, \lambda(t)) = R_1(t)\Gamma + R_2(t)^T T_c + R_0(t) \tag{21}$$

where

$$R_0(t) = \lambda_1(t)^T x_2(t) + \lambda_2(t)^T g, \qquad R_1(t) = \lambda_0 - \alpha \lambda_3(t)$$

$$R_2(t) = \frac{\lambda_2(t)}{m(t)}$$

and $x_2 \in \mathrm{IR}^3$ contains the velocity components of the vector, $x \in \mathrm{IR}^6$. Since $\lambda_2(t) \ne 0$, a.e. on $[0, t_f^*]$, $m^*(t) > 0$, and H depends linearly on T_c, the pointwise maximum principle given by (18) implies that, for the optimal solution,

$$\|T_c^*(t)\| = \Gamma^*(t), \qquad \text{a.e. on } [0, t_f^*] \tag{22}$$

This also implies that

[§]Here almost everywhere (a.e.) on $[0, t_f]$ means that the condition is valid on a set of points in the interval with an exception of a set of points with measure zero [25]. For simplicity, a.e. on $[0, t_f^*]$ can be replaced by $\forall \ t \in [0, t_f^*]$.

$$\rho_1 \le \|T_c^*(t)\| \le \rho_2, \qquad \text{a.e. on } [0, t_f^*]$$

Therefore, since an optimal solution of Problem 2 satisfies all the constraints of Problem 1 (even though the set of feasible controls of Problem 1 is strictly contained in the set of feasible controls of Problem 2), it also defines an optimal solution for Problem 1.

Now we will prove that $\|T_c^*(t)\| = \rho_1$ or $\|T_c^*(t)\| = \rho_2$ for any $t \in [0, t_f^*]$ by using the pointwise maximum principle with

$$H(\psi(t)) = R_{12}(t)\Gamma^*(t) + R_0(t), \quad \text{where } R_{12}(t) = R_1(t) + \|R_2(t)\|$$

The pointwise maximum principle implies that

$$\Gamma^*(t) = \begin{cases} \rho_1, & \text{if } R_{12}(t) < 0 \\ \rho_2, & \text{if } R_{12}(t) > 0 \end{cases}$$

To show $R_{12}(t) \neq 0$, a.e. on $[0, t_f^*]$, note that

$$\dot{R}_1 = -\frac{\alpha}{m}\|R_2\|\Gamma^*$$

which is obtained by using that $T_c^* = R_2\Gamma^*/\|R_2\|$ ($\|R_2\| \neq 0$ almost everywhere on $[0, t_f^*]$). Also, by noting that $\lambda_2 = mR_2$, we have

$$\frac{\mathrm{d}\|R_2\|}{\mathrm{d}t} = \frac{1}{m}\frac{\mathrm{d}\|\lambda_2\|}{\mathrm{d}t} + \frac{\alpha}{m}\|R_2\|\Gamma^*$$

Then,

$$m\dot{R}_{12} = \frac{\mathrm{d}}{\mathrm{d}t}\|\lambda_2\| = -\frac{1}{2\|\lambda_2\|}\lambda_2^T\lambda_1 = \frac{1}{2\|\lambda_2\|}(\|\lambda_1\|^2 t - \lambda_1^T a)$$

where λ_1 and a are constant vectors and they cannot be both zeros because λ_2 cannot be identically zero in time. Since $m > 0$, this clearly implies that $\dot{R}_{12}$ can not be identically zero when $\lambda_1 \neq 0$. When $\lambda_1 \neq 0$, it is also clear that $\dot{R}_{12}$ can be zero only at one point in time and the sign of $\dot{R}_{12}$ can only change from negative to positive. This implies that $R_{12}(t) \neq 0$ a.e. on $[0, t_f]$ when $\lambda_1 \neq 0$.

Now, note that $\dot{R}_{12}(t) = 0$ on some interval $[t_a, t_b] \subset [0, t_f]$ only if $\lambda_1 = 0$. In this case, $\dot{R}_{12}(t) = 0$ for all $t \in [0, t_f]$. Therefore, we have to show that $R_{12}(t) \neq 0$ when $\lambda_1 = 0$ to complete the proof. To do this, suppose that $R_{12} = 0$ as well as $\lambda_1 = 0$. These imply that λ_2 is constant in time, and $R_0(t) = g^T\lambda_2 = 0$ [because $H(\phi(t_f^*)) = 0$]. Since $T_c^* = R_2\Gamma^*/\|R_2\| = \lambda_2\Gamma^*/\|\lambda_2\|$, this implies that $g^T T_c^* = 0$ and there exists some positive scalars β_1 and β_2

$$0 = r_0 + gt_f^2/2 + \dot{r}_0 t_f + \beta_1\hat{n} \qquad 0 = \dot{r}_0 + gt_f + \beta_2\hat{n}$$

where $\hat{n} = \lambda_2/\|\lambda_2\|$. By premultiplying the preceding equalities with $-g/\|g\|$, we obtain

$$0 = r_{0_1} - \hat{g}t_f^2/2 + \dot{r}_{0_1}t_f \qquad 0 = \dot{r}_{0_1} - \hat{g}t_f$$

where $\hat{g} = \|g\|$, and r_{0_1} and $\dot{r}_{0_1}$ are the initial position and velocity components along the axis opposite to the direction of the gravity. This implies that

$$r_{0_1} = -\dot{r}_{0_1}^2/2\hat{g} \le 0 \quad \text{and} \quad \dot{r}_{0_1} \ge 0$$

Since $r_{0_1} > 0$ [see inequality (6)], this leads to a contradiction. Consequently, $R_{12}(t) \neq 0$ for $t \in [0, t_f]$ when $\lambda_1 = 0$. This completes the proof. □

Lemma 1 implies that the main nonconvex constraint on the thrust magnitude (3) in Problem 1 is convexified by replacing it with (14) and (15) in Problem 2 via the introduction of a scalar slack variable Γ. Furthermore, Lemma 1 presents a relation between the optimal solutions of Problem 1 and Problem 2. It states that if there exists an optimal solution for Problem 2, then there also exists one for Problem 1 and it can be obtained directly from the optimal solution of Problem 2. Also, note that the set of admissible controls of Problem 2 strictly contains the set of admissible controls of Problem 1. Consequently, one can solve Problem 2 with convex control constraints to obtain the solution of Problem 1 with nonconvex control constraints. See Fig. 3 for an illustration of the constraint convexification in a 2-D control space: The nonconvex constraint set for the control input, represented by the shaded annulus, is mapped into a convex set, represented by the cone, via the slack variable Γ.

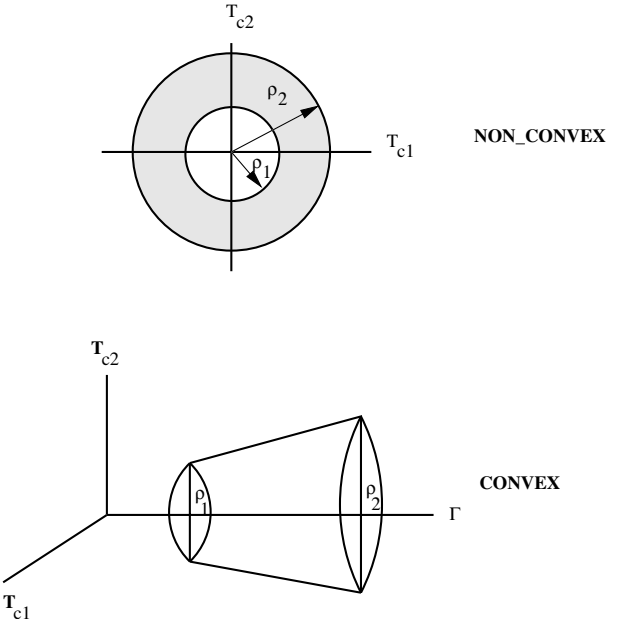

Fig. 3 Convexification of thrust magnitude constraint.

Remark 4: The thrust direction constraints at the start and end of a maneuver given by (12) can be described by using the fact that $\|T_c(t)\| = \Gamma(t)$, $t \in [0, t_f]$ for an optimal solution, as follows:

$$T_c(0) = \Gamma(0)\hat{n}_0, \qquad T_c(t_f) = \Gamma(t_f)\hat{n}_f \tag{23}$$

where $\hat{n}_0$ and $\hat{n}_f$ are described in (12). □

A. Existence of an Optimal Solution

At this point we have to solve Problem 2 to obtain an optimal solution for the minimum fuel trajectory optimization problem. An important theoretical issue is the existence of an optimal solution for Problem 2. In this section, we address this question of existence of an optimal solution. We first introduce some notation that will useful in this section. Let $\mathcal{F}$ represent the set of all feasible state and control signals for Problem 2, that is, $[x(\cdot), m(\cdot), T_c(\cdot), \Gamma(\cdot)] \in \mathcal{F}$ implies that, for $t \in [0, t_f]$, $[x(t), m(t)]$ and $[T_c(t), \Gamma(t)]$ define a feasible state trajectory and control signal for Problem 2. A more general form of the following existence theorem and its proof can be found in p. 61 of [23].

Theorem 1: Consider the following optimal control problem:

$$\min_{v(\cdot)} J(y(\cdot), u(\cdot), t_f) = \int_0^{t_f} g(y(t), u(t))\,\mathrm{d}t$$

$$\text{subject to } \dot{y}(t) = f(y(t), v(t))$$

$$y(t) \in \mathcal{Y} \quad \text{and} \quad v(t) \in \mathcal{V} \quad \forall\ t \in [0, t_f]$$

$$y(0) \in B_0 \quad \text{and} \quad y(t_f) \in B_f$$

Suppose the set of all feasible state trajectories and control signals, $\mathcal{F}$, for this problem is nonempty. Furthermore suppose that 1) there exists a compact set $\mathcal{R}$ such that all feasible state trajectories satisfy $[t, y(t)] \in \mathcal{R}$ for all $t \in [0, t_f]$; 2) the set of all feasible $[y(0), t_f, y(t_f)]$, such that $y(0) \in B_0$ and $y(t_f) \in B_f$, is closed; 3) the set $\mathcal{V}$ is compact; 4) $[g, f^T]^T$ is a continuous vector valued function on $\mathcal{Y} \times \mathcal{V}$; and 5) for each $(t, y) \in \mathcal{R}$, $Q^+(t, y)$ is convex, where

$$Q^+(y) = \{(z_1, z_2)\colon z_1 \ge g(y, v), z_2 = f(y, v), v \in \mathcal{U}\} \tag{24}$$

Then there exists a feasible state and control signal pair $[y^*(\cdot), u^*(\cdot)]$ such that

$$J(y^*(\cdot), u^*(\cdot), t_f^*) \le J(y(\cdot), u(\cdot), t_f) \quad \forall\ [y(\cdot), u(\cdot)] \in \mathcal{F}$$

Note that there is no constraint on the final time (time of flight) t_f in Problem 2. However, because there is limited fuel onboard a spacecraft, there is an upper bound on time of flight $t_{\max}$. Therefore, we will only consider feasible solutions with $t_f \in [0, t_{\max}]$ for the rest of the discussion. Given this upper bound on t_f and the fact that all the feasible position and velocity vectors, the spacecraft mass, and the control inputs are in compact sets, guarantees the satisfaction of first three conditions of Theorem 1 by Problem 2. The fourth condition is also satisfied. Now we show that the fifth condition is also satisfied, which demonstrates the existence of an optimal solution when the set of feasible solutions is nonempty. To do that, note that we have the following for Problem 2:

$$\begin{aligned} Q^+(x, m) = \{&(z_1, z_2, z_3, z_4), z_1 \text{ and } z_4 \in \mathrm{IR}, z_2, \text{ and } z_3 \in \mathrm{IR}^3\colon z_1 \\ &\ge \Gamma, (z_2, z_3, z_4) = (x_2, g + T_c/m, -\alpha\Gamma), \rho_1 \le \Gamma \le \rho_2, \|T_c\| \\ &\le \Gamma\} \end{aligned}$$

This implies that $(z_1, z_2, z_3, z_4) \in Q^+(t, x, m)$ if and only if it satisfies

$$\begin{gathered} z_1 \ge -z_4/\alpha, \qquad z_4 = -\alpha\Gamma, \qquad z_3 = g + T_c/m, \qquad z_2 = x_2 \\ -z_4 \ge \alpha\|T_c\|, \qquad \alpha\|(z_2 - g)m\| \le -z_4, \qquad \|T_c\| \le \Gamma \\ \rho_1 \le \Gamma \le \rho_2 \end{gathered}$$

Since all of the preceding equalities are linear, and the inequalities are either linear or second-order cone constraints, the set $Q^+(x, m)$ is convex. By using Theorem 1, this concludes that Problem 2 has an optimal solution when it has a feasible one.

B. Change of Variables

In this section we introduce a change of variables that will be useful in constructing the numerical solution algorithm for Problem 2. The change of variables will lead to Problem 3 (given later in this section) that is a continuous-time optimal control problem with a convex cost and convex state and control constraints; particularly with second-order cone or linear state and control constraints.

Consider the following change of variables:

$$\sigma \triangleq \frac{\Gamma}{m} \quad \text{and} \quad u \triangleq \frac{T_c}{m} \tag{25}$$

Equations (1) and (13) can then be rewritten as

$$\ddot{r}(t) = u(t) + g \tag{26}$$

$$\frac{\dot{m}(t)}{m(t)} = -\alpha\sigma(t) \tag{27}$$

From Eq. (27),

$$m(t) = m_0 \exp\left[-\alpha \int_0^{t_f} \sigma(\tau)\, \mathrm{d}\tau\right]$$

Because $\alpha > 0$, minimizing fuel [or maximizing $m(t_f)$] is equivalent to minimizing

$$\int_0^{t_f} \sigma(t)\, \mathrm{d}t$$

The control constraints are expressed in terms of the new variables u and σ as follows:

$$\|u(t)\| \le \sigma(t), \quad \forall\ t \in [0, t_f] \tag{28}$$

$$\frac{\rho_1}{m(t)} \le \sigma(t) \le \frac{\rho_2}{m(t)}, \quad \forall\ t \in [0, t_f] \tag{29}$$

Remark 5: When we consider Problem 2 with the new variables, the following is satisfied for any pair of optimal controls u^* and σ^*:

$$\|u^*(t)\| = \sigma^*(t), \quad \forall\ t \in [0, t_f^*]$$

□

Note that the inequalities in (29) define a convex region for the control input u for a prescribed mass profile $m(t)$ on $[0, t_f]$. However, when we consider m as a variable of the problem, these inequalities become bilinear, and hence they define nonconvex constraints. The following variable is introduced to resolve this issue and convexify the inequalities in (29):

$$z \triangleq \ell_n\, m \tag{30}$$

Then Eq. (27) is written as

$$\dot{z}(t) = -\alpha\sigma(t) \tag{31}$$

and the inequalities in (29) become

$$\rho_1 e^{-z(t)} \le \sigma(t) \le \rho_2 e^{-z(t)}, \quad \forall\ t \in [0, t_f] \tag{32}$$

The first part of inequality (32) defines a convex feasible region, but the second part does not. Here, we obtain second-order cone or linear approximations of these inequalities that can be readily incorporated into our solution framework. To do that, we use the Taylor series expansion of e^{-z}. The first part of inequality (32) can be approximated by a second-order cone (by using the first three terms of the Taylor series expansion of e^{-z}) as

$$\rho_1 e^{-z_0}\left[1 - (z - z_0) + \frac{(z - z_0)^2}{2}\right] \le \sigma$$

where z_0 is a given constant. For the second part of inequality (32), we use a linear approximation of e^{-z} (by using the first two terms of the Taylor series expansion of e^{-z}) to obtain

$$\sigma \le \rho_2 e^{-z_0}[1 - (z - z_0)]$$

Letting

$$\mu_1 \triangleq \rho_1 e^{-z_0}, \qquad \mu_2 \triangleq \rho_2 e^{-z_0} \tag{33}$$

we obtain the following second-order cone and linear approximations of the inequalities in (32):

$$\begin{aligned} \mu_1(t)\left[1 - [z(t) - z_0(t)] + \frac{[z(t) - z_0(t)]^2}{2}\right] &\le \sigma(t) \\ \le \mu_2(t)\{1 - [z(t) - z_0(t)]\}, \quad \forall\ t \in [0, t_f]& \end{aligned} \tag{34}$$

where

$$z_0(t) = \ell_n(m_{\text{wet}} - \alpha\rho_2 t) \tag{35}$$

and m_{wet} is the initial mass of the spacecraft, that is, $z_0(t)$ is a lower bound on $z(t)$ at time t. To ensure that the physical bounds on z are not violated, we impose the additional constraints

$$\ell_n(m_{\text{wet}} - \alpha\rho_2 t) \le z(t) \le \ell_n(m_{\text{wet}} - \alpha\rho_1 t) \tag{36}$$

An approximation of Problem 2 can now be expressed in terms of the new control variables:

Problem 3:

$$\min_{t_f,u(\cdot),\sigma(\cdot)} \int_0^{t_f} \sigma(t)\,\mathrm{d}t \qquad \text{subject to } \ddot{r}(t) = u(t) + g$$

$$\dot{z}(t) = -\alpha\sigma(t), \qquad \|u(t)\| \le \sigma(t)$$

$$\mu_1(t)\left[1 - [z(t) - z_0(t)] + \frac{[z(t) - z_0(t)]^2}{2}\right] \le \sigma(t)$$

$$\le \mu_2(t)\{1 - [z(t) - z_0(t)]\}$$

$$\ell_n(m_{\text{wet}} - \alpha\rho_2 t) \le z(t) \le \ell_n(m_{\text{wet}} - \alpha\rho_1 t)$$

$$\|S_j x(t) - v_j\| + c_j^T x(t) + a_j \le 0, \qquad j = 1, \ldots, n_s$$

$$m(0) = m_{\text{wet}}, \qquad r(0) = r_0, \qquad \dot{r}(0) = \dot{r}_0$$

$$r(t_f) = \dot{r}(t_f) = 0$$

where α, ρ_1, ρ_2, S_j, a_j, c_j, r_0, $\dot{r}_0$ are constant parameters defined in (1–5) and (8), and μ_1 and μ_2 are functions defined by (33). □

Remark 6: In Problem 3, the thrust direction constraints at the start and end of a maneuver given by (23) can be described by using the new control variables as follows:

$$u(0) = \sigma(0)\hat{n}_0, \qquad u(t_f) = \sigma(t_f)\hat{n}_f \tag{37}$$

where $\hat{n}_0$ and $\hat{n}_f$ are described in (12). □

The approximation of inequalities (32) given by (34) and (36) is generally very accurate for both parts of the inequality. Actually we can compute bounds on the errors introduced by these approximations. To do that, first we use the following relationship for the Taylor series expansion [26] of e^{-z}: For any $z \in [z_0, z_u]$, where $z_u = \ell_n(m_{\text{wet}} - \alpha\rho_1 t)$, there exists $\bar{z} \in [z_0, z_u]$ such that

$$e^{-z} = e^{-z_0}\left[1 - (z - z_0) + \frac{(z - z_0)^2}{2}\right] - \underbrace{e^{-\bar{z}}\frac{(z - z_0)^3}{6}}_{\triangleq a(z)}$$

Letting $p_{e1}(t) = 100a(z(t))/e^{-z(t)}$ (percent approximation error) and using $z = \ell_n m$, we have

$$p_{e1}(t) = \frac{50m(t)\,\ell_n[m(t)/m_0(t)]^3}{3\bar{m}(t)}$$

where $\bar{m}(t) = e^{-\bar{z}(t)}$, $m_0 = e^{-z_0(t)}$. Note that, for any given time t,

$$\bar{m}(t), m(t) \in [m_0(t), m_u(t)] \quad \text{where } m_0(t) = m_{\text{wet}} - \alpha\rho_2 t$$

$$m_u(t) = m_{\text{wet}} - \alpha\rho_1 t$$

This implies the following bounds on the percent approximation error for the left-hand side of inequality (32):

$$0 \le p_{e1}(t) \le \frac{50m_u(t)}{3m_0(t)}\,\ell_n\left(\frac{m_u(t)}{m_0(t)}\right)^3 \tag{38}$$

By using similar steps, we can also establish a bound on the percent error for the right-hand side of inequality (32), which is denoted by p_{e2},

$$0 \le p_{e2}(t) \le \frac{50m_u(t)}{m_0(t)}\,\ell_n\left(\frac{m_u(t)}{m_0(t)}\right)^2 \tag{39}$$

Figure 4 presents an example showing the accuracy of the approximations on an example problem that will be introduced later in the paper. In this figure, we compute the maximum percent error as a function of time, that is: Given $0 \le t \le t_f$, we compute the bounds on the errors p_{e1} and p_{e2} that are given by inequalities (38) and (39). The figure clearly shows that the inequalities (32) are not compromised for all practical purposes when they are approximated by inequalities (34) and (36).

Furthermore, the following lemma establishes the fact that, if there exists a solution of Problem 3, then there exists a solution of the problem with inequalities (34) and (36) replaced by inequalities (32). Therefore, by solving Problem 3, one never obtains solutions which violate the constraints of the physical problem.

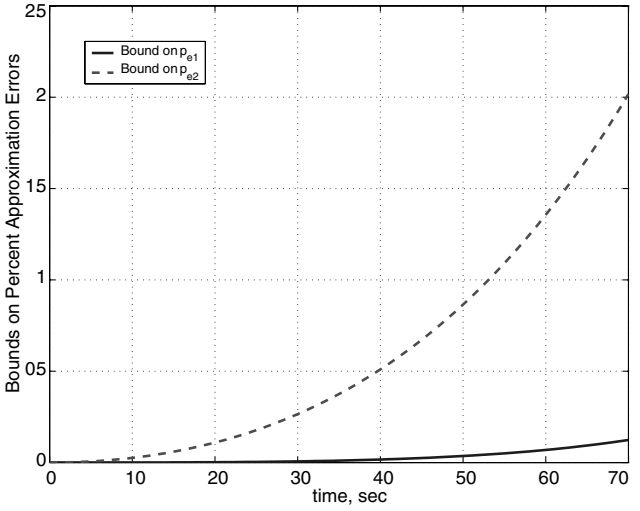

Fig. 4 Error bounds for the approximation of e^z.

Lemma 2: If there exists a feasible solution of Problem 3, then this solution also defines a feasible solution of Problem 3 when inequalities (34) and (36) are replaced by inequalities (32), that is, when the exact control magnitude constraint is imposed.

Proof: The only difference between the two optimization problems is the approximation of constraint (32) by (34) and (36). To prove the claim of the lemma, we only have to show that the interval on the real line defined by (32) contains the interval defined by (34) and (36) for all t. For that, first consider the lower bound in (32), where e^{-z} is approximated by a Taylor series up to quadratic terms around z_0, where z_0 is a known lower bound on z from constraint (36). Because e^{-z} has continuous derivatives, we have the following by using the Mean Value theorem [26]:

$$e^{-z} = e^{-z_0}\left[1 - [z(t) - z_0(t)] + \frac{[z(t) - z_0(t)]^2}{2}\right] - e^{-\hat{z}}\frac{[z(t) - z_0(t)]^3}{6}$$

where $\hat{z} \in [z_0, z]$. This implies that

$$e^{-z_0}\left[1 - [z(t) - z_0(t)] + \frac{[z(t) - z_0(t)]^2}{2}\right] \ge e^{-z}$$

The preceding inequality shows that the lower bound in (34) is larger than the lower bound in (32).

To prove the claim on the upper bounds, we use similar arguments by noting that

$$e^{-z} = e^{-z_0}\{1 - [z(t) - z_0(t)]\} + e^{-\hat{z}}\frac{[z(t) - z_0(t)]^2}{2}$$

for some $\hat{z} \in [z_0, z]$. This implies that

$$e^{-z_0}\{1 - [z(t) - z_0(t)]\} \le e^{-z}$$

which proves that the upper bound in (34) is smaller than the upper bound in (32). This completes the proof. □

IV. Discretization of Problem 3 and a Solution Algorithm

In this section, we apply a discretization to Problem 3, and develop a numerical algorithm to solve the resulting discrete version of the problem. The discretization of Problem 3 converts the infinite-dimensional optimization problem to a finite-dimensional one by discretizing the time domain into equal time intervals and imposing

the constraints at the temporal nodes. Because the constraints are linear or second-order cone constraints, the resulting problem is a finite-dimensional SOCP problem that can be efficiently solved by readily available algorithms [17–19].

For any given time interval $[0, t_f]$, and time increment, Δt, the temporal nodes are given as

$$t_k = k\Delta t, \qquad k = 0, \ldots, N$$

where $N\Delta t = t_f$. The second step in the discretization of the problem is the representation of the control input u and σ in terms of some prescribed basis functions, $\phi_1, \ldots, \phi_M$,

$$\begin{bmatrix} u(t) \\ \sigma(t) \end{bmatrix} = \sum_{j=1}^{M} p_j \phi_j(t), \qquad t \in [0, t_f] \tag{40}$$

where $p_j \in \mathrm{IR}^4$ are constant coefficients. The solution of the differential Eqs. (26) and (31), and the control input u at the temporal nodes can be expressed in terms of these coefficients as

$$\begin{bmatrix} x(t_k) \\ z(t_k) \end{bmatrix} = \xi_k + \Psi_k \eta, \qquad k = 1, \ldots, N \tag{41}$$

$$\begin{bmatrix} u(t_k) \\ \sigma(t_k) \end{bmatrix} = \Upsilon_k \eta, \qquad k = 0, \ldots, N \tag{42}$$

where

$$\xi_k = \Phi_k y_0 + \Lambda_k \begin{bmatrix} g \\ 0 \end{bmatrix} \tag{43}$$

Φ_k, Ψ_k, Λ_k, Υ_k, and Ω_k are matrix functions of time index determined by the basis functions chosen, and

$$\eta = \begin{bmatrix} p_1 \\ \vdots \\ p_M \end{bmatrix}, \qquad y_0 = \begin{bmatrix} r_0 \\ \dot{r}_0 \\ \ell_n\, m_{\text{wet}} \end{bmatrix}, \qquad x(t_k) = \begin{bmatrix} r(t_k) \\ \dot{r}(t_k) \end{bmatrix} \tag{44}$$

In this paper, we use piecewise constant basis functions in our simulations,

$$\phi_j(t) = \begin{cases} 1 & \text{when } t \in [t_{j-1}, t_j) \\ 0 & \text{otherwise} \end{cases}, \qquad j = 1, \ldots, N \tag{45}$$

which implies that $M = N$ and

$$p_j = \begin{bmatrix} u(t_{j-1}) \\ \sigma(t_{j-1}) \end{bmatrix}, \qquad j = 1, \ldots, N \tag{46}$$

This corresponds to zero-order-hold discretization of a linear time invariant system for the dynamics of the spacecraft (26) and (31), with the vector $[r(t_k)^T, \dot{r}(t_k)^T, z(t_k)^T]^T$ as the state, and $(A, B) \in (\mathrm{IR}^{7\times 7}, \mathrm{IR}^{7\times 4})$ as the matrix pair describing the discrete time dynamics, which are given by

$$A = e^{A_c \Delta t}$$

$$B = \int_0^{\Delta t} e^{A_c(\Delta t - s)} B_c \, \mathrm{d}s \quad \text{where } A_c = \begin{bmatrix} 0 & I & 0 \\ 0 & 0 & 0 \\ 0 & 0 & 0 \end{bmatrix}$$

$$B_c = \begin{bmatrix} 0 & 0 \\ I & 0 \\ 0 & -\alpha \end{bmatrix}$$

Consequently,

$$\Phi_k = A^k, \qquad \Lambda_k = B + AB + \cdots + A^{k-1}B$$

$$\Psi_k = \begin{bmatrix} 0 & 0 & \ldots & \ldots & 0 \\ B & 0 & \ldots & \ldots & 0 \\ B & AB & 0 & \ldots & 0 \\ \vdots & \vdots & \vdots & \vdots & \vdots \\ A^{k-1}B & \ldots & B & 0 & \ldots \\ 0 & 0 & \ldots & . & 0 \end{bmatrix}$$

$$\Upsilon_k = \begin{bmatrix} 0 & \ldots & 0 & I & 0 & \ldots \end{bmatrix}$$

Remark 7: Other basis functions such as Chebyshev polynomials [11,12,27] can also be used. Then, the description of the controls can be achieved with fewer number of coefficients $M \ll N$. This leads to significant reductions in the dimension of the resulting finite-dimensional SOCP, and in the execution times of the algorithm. In that case the preceding matrices will change but the resulting form of the optimization problem will be very close. Therefore, we choose a piecewise constant approximation of the control input as an example to demonstrate the discretization and the conversion of the optimal control problem into a parameter optimization problem. □

The cost of the trajectory optimization problem can also be approximated as follows:

$$\int_0^{t_f} \sigma(t)\, \mathrm{d}t \approx \sum_{k=1}^{M} w_k e_\sigma^T p_k \tag{47}$$

where w_k are scalar coefficients defined by the numerical integration technique and

$$e_\sigma = \begin{bmatrix} 0 & 0 & 0 & 1 \end{bmatrix}^T \tag{48}$$

If the basis functions for the control input are described by (45), then these coefficients can simply be chosen as $w_0 = \cdots = w_{N-1} = \Delta t$.

Each inequality constraint in Problem 3 can be expressed in a generic form as follows:

$$g(t, r(t), \dot{r}(t), u(t)) \le 0, \quad \forall\ t \in [0, t_f]$$

where g: $\mathrm{IR}^{10} \to \mathrm{IR}$ is an appropriately chosen function. If (41) and (42) are substituted in the aforementioned inequalities, we obtain

$$\tilde{g}(t_k, \eta) \le 0, \qquad k = 0, \ldots, N$$

for some function $\tilde{g}$: $\mathrm{IR}^{3M+1} \to \mathrm{IR}$. Note that the constraints are only satisfied at the temporal nodes in the discrete version of the optimization problem. Also, if g is a convex function of r, $\dot{r}$, and u, which depend linearly on η, then $\tilde{g}$ is a convex function of η.

Now, with the following additional notation, Problem 4 describes the discretized version of Problem 3,

$$\begin{gathered} E = \begin{bmatrix} I_{6\times 6} & 0_{6\times 1} \end{bmatrix}, \qquad F = \begin{bmatrix} 0_{1\times 6} & 1 \end{bmatrix} \\ \omega = \begin{bmatrix} w_1 e_\sigma^T & \ldots & w_M e_\sigma^T \end{bmatrix}^T, \qquad E_u = \begin{bmatrix} I_{3\times 3} & 0_{3\times 1} \end{bmatrix} \end{gathered} \tag{49}$$

Problem 4:

$$\min_{N,\eta} \ \omega^T \eta \qquad \text{subject to } \|E_u \Upsilon_k \eta\| \le e_\sigma^T \Upsilon_k \eta, \qquad k = 0, \ldots, N \tag{50}$$

$$\begin{gathered} \mu_1(t_k)\left[1 - \{F[\xi_k + \Psi_k\eta] - z_0(t_k)\} + \frac{\{F[\xi_k + \Psi_k\eta] - z_0(t_k)\}^2}{2}\right] \\ \le e_\sigma^T \Upsilon_k \eta \le \mu_2(t_k)(1 - \{F[\xi_k + \Psi_k\eta] - z_0(t_k)\}) \\ k = 1, \ldots, N \end{gathered} \tag{51}$$

$$\begin{gathered} \ell_n(m_{\text{wet}} - \alpha\rho_2 t_k) \le F[\xi_k + \Psi_k\eta] \le \ell_n(m_{\text{wet}} - \alpha\rho_1 t_k) \\ k = 1, \ldots, N \end{gathered} \tag{52}$$

$$\|S_j E[\xi_k + \Psi_k \eta] - v_j\| + c_j^T E[\xi_k + \Psi_k \eta] + a_j \le 0 \qquad k = 1, \ldots, N, \qquad j = 1, \ldots, n_s \tag{53}$$

□

Note that Problem 4 defines a finite-dimensional second-order cone program (SOCP) for any given N, and it can be solved very efficiently with guaranteed convergence to the globally optimal solution by using existing SOCP algorithms [14,15,17]. Here N describes the time of flight $t_f = N\Delta t$, and it is also a solution parameter in Problem 4. It is also clear that there exists bounds $0 < t_{\min} < t_{\max}$ such that

$$t_{\min} \le t_f \le t_{\max} \tag{54}$$

Actually some conservative bounds on t_f can easily be obtained as follows from the physical limitations imposed by the fuel mass m_{fuel}, maximum and minimum thrust levels ρ_2 and ρ_1, and initial velocity $\dot{r}(0)$:

$$t_{\min} = \frac{(m_{\text{wet}} - m_{\text{fuel}})\|\dot{r}(0)\|}{\rho_2}, \qquad t_{\max} = \frac{m_{\text{fuel}}}{\alpha \rho_1} \tag{55}$$

Because the time axis is discretized with a constant increment Δt, the bounds in (55) imply bounds on N, that is,

$$N_{\min} \le N \le N_{\max} \tag{56}$$

where

$$N_{\min} = \text{int}(t_{\min}/\Delta t) + 1, \qquad N_{\max} = \text{int}(t_{\max}/\Delta t) \tag{57}$$

and $\text{int}(t)$ gives the closest integer number to t and $\text{int}(t) \le t$.

Remark 8: The available fuel mass is not considered to be a constraint in the original trajectory optimization problem given by Problem 1. We introduce this constraint in the rest of the paper to account for this physical constraint as well as to obtain an upper bound on the time of flight. □

Remark 9: Here our objective is to obtain an optimal solution of Problem 2 (which is also an optimal solution of Problem 1) by numerically solving for an optimal solution of Problem 3. By Lemma 2, this solution satisfies all the constraints of Problem 2, which implies that it is a feasible solution of Problem 2. Note that, if a solution of Problem 3 is found then, by using Theorem 1, there exists an optimal solution of Problem 2. The difference between these two problems is the approximation of the inequalities (32) by (34) and (36), which is demonstrated to be very accurate for our purposes (see Fig. 4 and the accompanying discussion). Consequently, an optimal solution of Problem 3 is very close to an optimal solution of Problem 2.

An optimal solution of Problem 3 is obtained by solving SOCP described by Problem 4. Because Problem 4 describes an SOCP, its numerical solution obtained by using an interior-point method is guaranteed to be a globally minimizing solution [19]. Clearly Problem 4 is a numerical approximation of Problem 3 that becomes more accurate as the number of basis functions describing the control input increases and Δt decreases.¶ As a result, an optimal solution of Problem 4 describes a feasible solution of Problem 2 that is very close to an optimal solution of this problem for all practical purposes. □

The following algorithm gives a numerical approach to obtain the solution of Problem 4:

Algorithm 1: Apply a *line search* on positive integers $N \in [N_{\min}, N_{\max}]$ to minimize $\beta(N)$, where $\beta(N)$ is defined by the solution of Problem 4 for a given N as follows: Let

$$\mathcal{F}_N = \{\eta \in \text{IR}^{4N}\text{: (50), (51), (52), (53) hold for } \eta\}$$

then

$$\beta(N) = \begin{cases} \infty, & \text{if } \mathcal{F}_N \text{ is empty} \\ \min\limits_{\eta \in \mathcal{F}_N} \omega^T \eta, & \text{if } \mathcal{F}_N \text{ is nonempty} \end{cases} \tag{58}$$

The line search gives the optimum solution pair (N_*, η_*) and corresponding $\beta_* = \beta(N_*)$, and

1) If $(1 - e^{-\alpha\beta_*})m_{\text{wet}} \le m_{\text{fuel}}$, the pair (N_*, η_*) defines a valid solution.

2) If $(1 - e^{-\alpha\beta_*})m_{\text{wet}} > m_{\text{fuel}}$, then:

a) If $\beta_* < \infty$, there is no feasible solution of Problem 4 due to insufficient fuel.

b) If $\beta_* = \infty$, there is no feasible solution of Problem 4 due to insufficient thrusters. □

Remark 10: In [2], it is shown that the minimum fuel and the minimum time optimal solutions of a 1-D version of the soft-landing problem are identical. We have a similar observation from our simulations that the optimal time of flight $t_f^* = N_* \Delta t$ obtained from Algorithm 1 is usually very close to the minimal feasible time of flight for Problem 4, and the fuel cost is unimodal function (see [28] for a definition of unimodal functions) of the time of flight. This observation is used to efficiently implement the line search in Algorithm 1 for the optimal time of flight. □

V. Powered Descent Guidance Example

In this section, we present some powered descent examples for Mars pinpoint landing. The simulations are carried out by using SeDuMi [17,19] with a MATLAB interface.** The problem parameters are

$$g = [-3.7114\,0\,0]^T \text{ m/s}^2 \qquad m_{\text{dry}} = 1505 \text{ kg}$$
$$m_{\text{wet}} = 1905 \text{ kg} \qquad I_{\text{sp}} = 225 \text{ s}, \qquad \bar{T} = 3.1 \text{ kN} \tag{59}$$
$$T_1 = 0.3\bar{T}, \qquad T_2 = 0.8\bar{T}, \qquad n = 6, \qquad \phi = 27 \text{ deg}$$

where $\bar{T}$ is the maximum thrust for each thruster. In the simulation results given in Figs. 5 and 6, we present the time histories of the velocity, position, acceleration, net thrust force components, throttle level (which is between 0.3 and 0.8 in this case), and the angle between the net thrust direction and the direction of gravity θ. An additional constraint on the thrust direction at the final time t_f is imposed to be the opposite direction to the gravity vector, that is, the second equality in (37) is imposed with

$$\hat{n}_f = \begin{bmatrix} 1 & 0 & 0 \end{bmatrix}^T$$

First we present a simulation, in which the constraint given by (7) is not implemented, in Fig. 5. The constraint given by (7) ensures that the spacecraft does not fly subsurface. The position time history given in Fig. 5 shows that the spacecraft actually flies subsurface in $t \in (25, 50)$ when constraint (7) is not imposed. This example is then repeated by imposing this constraint, and the results in Fig. 6 show that the subsurface flight is eliminated. Also, a *max-min-max* type net optimal thrust profile is observed from the simulation results, which is a characteristic of the minimum fuel trajectories that is also implied by Lemma 1. However, the trajectory touches the surface, that is, $x(t_*) = 0$ for some $t_* \in (30, 40)$ seconds as observed in Fig. 6. This is not a practically acceptable solution even though it satisfies no-subsurface flight constraint. A practical approach to solve this problem is to introduce a glide slope constraint given by inequality (11) with $\tilde{\theta}_{\text{alt}} = 86$ deg. The simulation results with the glide slope constraint are given in Figs. 7 and 8, in which Fig. 8 shows the actual trajectory with the glide slope constraint boundary. Clearly, the optimal trajectory satisfies the control and the state constraints.

¶A more rigorous mathematical discussion on the approximation of Problem 3 via Problem 4 as the number of basis functions increases and Δt decreases is beyond the scope of this paper.

**Data available online at http://control.ee.ethz.ch/joloef/yalmip.msql [retrieved 1 May 2004].

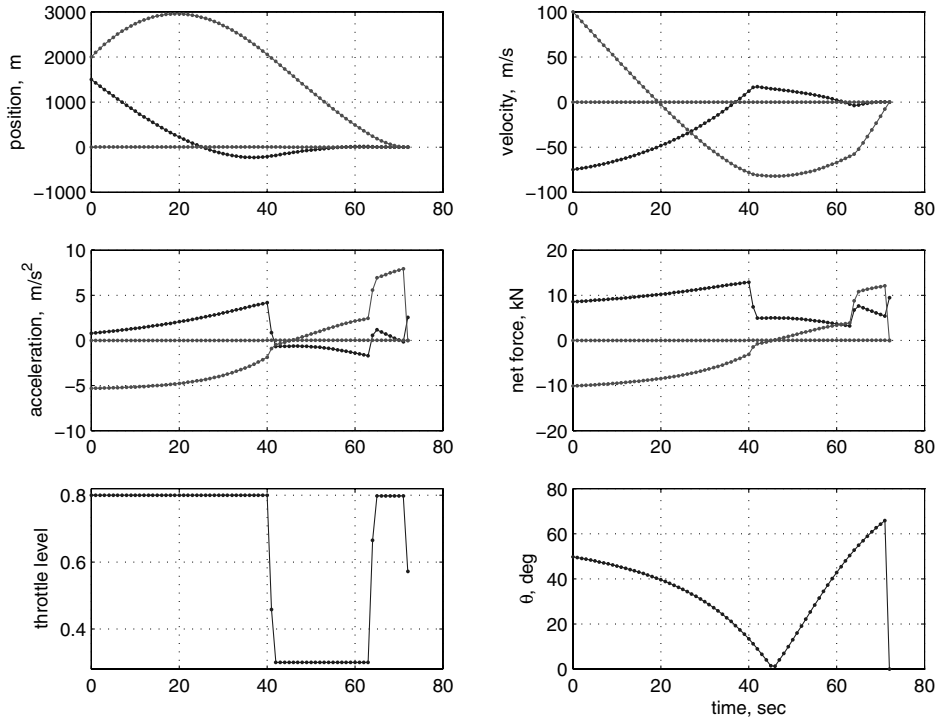

Fig. 5 $r_0 = [1.5, 0, 2]^T$ km, $\dot{r}_0 = [-75, 0, 100]^T$ m/s, $t_f^* = 72$ s, fuel usage = 387.9 kg without no-subsurface flight constraint.

VI. Trajectory Optimization with Thrust Pointing Constraints

In this section, we introduce an additional control constraint that is imposed by the constraints on the spacecraft attitude. In the translational trajectory optimization problem the spacecraft is treated as a point mass with a single thrust vector (representing the net thrust) attached to it. This simplification is based on the assumption that the net thrust on the spacecraft can be pointed arbitrarily to any given direction and the only constraint is on the thrust magnitude. However, in reality, there can be additional constraints on the spacecraft attitude that put constraints on the pointing of the net thrust direction. For example, there can be a camera onboard that has to be directed to the ground for a majority of the time during the maneuver. This may imply that the thrust direction must not deviate more than θ degrees from the positive x direction (see Fig. 1 for the definition of positive x direction), where $\theta \in [0 \text{ deg}, 180 \text{ deg}]$. This type of constraint can easily be expressed in our framework as follows:

$$\frac{v^T T_c(t)}{\|T_c(t)\|} \geq \gamma \quad \forall\ t \in [0, t_f] \tag{60}$$

where $\gamma = \cos\theta$ and $v \in \mathrm{IR}^3$ is a unit vector defining the cone that

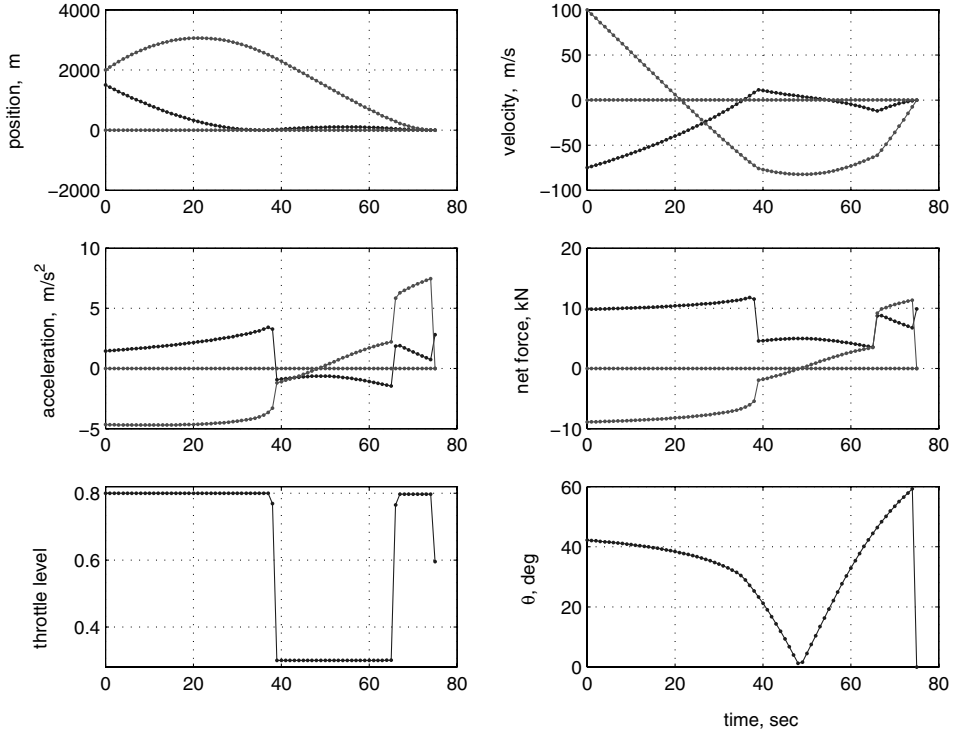

Fig. 6 $r_0 = [1.5, 0, 2]^T$ km, $\dot{r}_0 = [-75, 0, 100]^T$ m/s, $t_f^* = 75$ s, fuel usage = 390.4 kg with no-subsurface flight constraint.

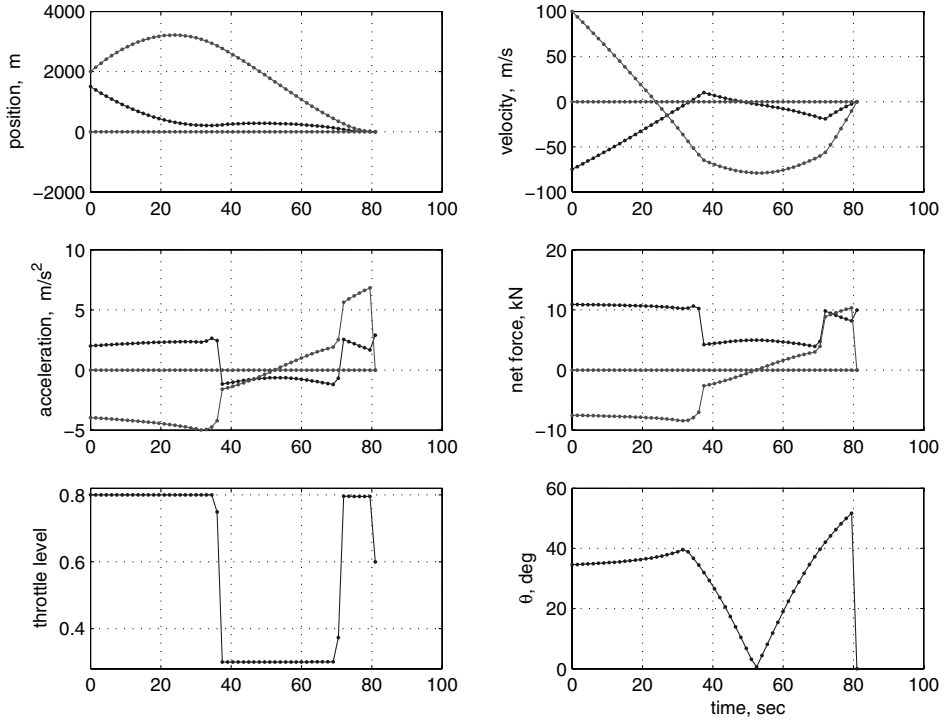

Fig. 7 $r_0 = [1.5, 0, 2]^T$ km, $\dot{r}_0 = [-75, 0, 100]^T$ m/s, $t_f^* = 81$ s, fuel usage = 399.5 kg with glide slope constraint.

the thrust vector must point into. This constraint can now be expressed by the solution variables as follows:

$$v^T u(t) \geq \gamma \sigma(t) \quad \forall\ t \in [0, t_f] \tag{61}$$

Clearly, the additional constraint on the thrust vector defines a convex region in IR^3 that can readily be expressed as a second-order cone constraint. However, the whole convexification of the problem depends on Lemma 1 where the nonconvex control magnitude constraints are convexified via a lossless relaxation (the relaxation still leads to the optimal solution of the original problem). From the proof of Lemma 1, if we do not have a thrust pointing constraint, the following holds for the optimal solution of Problem 2 (the relaxed problem):

$$u(t) = \sigma(t) \frac{R_2(t)}{\|R_2(t)\|}$$

where $R_2(t)$ is as defined in the proof of Lemma 1. This follows from the application of Maximum Principle with the following Hamiltonian (refer to the proof of Lemma 1 for the definitions of variables):

$$H(t) = R_1(t)m(t)\sigma(t) + m(t)R_2(t)^T u(t) + R_0(t)$$

However, when the thrust pointing constraint exists and if, for some t,

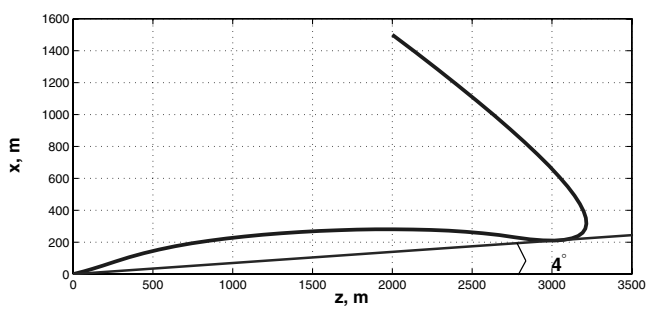

Fig. 8 $r_0 = [1.5, 0, 2]^T$ km, $\dot{r}_0 = [-75, 0, 100]^T$ m/s, $t_f^* = 81$ s, fuel usage = 399.5 kg with glide slope constraint.

$$\xi^T \frac{R_2(t)}{\|R_2(t)\|} \leq 0 \quad \forall\ \xi \text{ satisfying } v^T \xi \geq \gamma \quad \text{and} \quad \|\xi\| = 1$$

the optimal solution of Problem 2 must satisfy

$$\|u(t)\| = 0$$

which is the solution that maximizes the Hamiltonian without violating the control constraints of Problem 2. This violates the minimum thrust magnitude constraint of the original problem, Problem 1. Consequently, a convex equivalent of Problem 1 is not given by Problem 2 when such thrust direction constraint exists. Here, we introduce a heuristic approach to resolve this issue on the numerical approximation of Problem 2 that is given by Problem 4. Problem 4 is first solved without enforcing the thrust pointing constraint. This solution gives

$$\hat{r}_k \triangleq R_2(t_k)/\|R_2(t_k)\| = u_k/\|u_k\|$$

at the temporal points. This solution is then used to implement the pointing constraint by relaxing it when necessary (i.e., when it can not be simultaneously satisfied with the thrust magnitude constraint) with the following approach: Let

$$\kappa_{1,k} \triangleq v^T \hat{r}_k \quad \text{and} \quad \kappa_{2,k} \triangleq \|v - (v^T \hat{r}_k)\hat{r}_k\|$$

1) If $\kappa_{1,k} \geq 0$ or $\kappa_{2,k} \geq \gamma$, implement the thrust pointing constraint at temporal index k as it is given by inequality (61). There is no relaxation in this case, and the pointing constraint is enforced exactly.

2) If $\kappa_{1,k} < 0$ and $\kappa_{2,k} < \gamma$, then implement the following relaxed version of the thrust pointing constraint:

$$v^T u_k \geq \kappa_{2,k} \sigma(t) \tag{62}$$

This approach is motivated by the assumption that $\hat{r}_k$ is a good approximation for $R_2(t_k)/\|R_2(t_k)\|$. To demonstrate the idea behind this heuristic, consider the set $D_k = \{\xi\colon \|\xi\| = 1, \hat{r}_k^T \xi \geq 0 \text{ and } v^T \xi \geq \gamma\}$. If $\hat{r}_k$ is a good approximation for $R_2(t_k)/\|R_2(t_k)\|$, then Problem 2 has an optimal control at t_k that does not violate the minimum thrust magnitude constraint only if D_k is nonempty. If $\kappa_{1,k} \geq 0$, then $v \in D_k$, that is, D_k is nonempty. Suppose that $\kappa_{1,k} < 0$

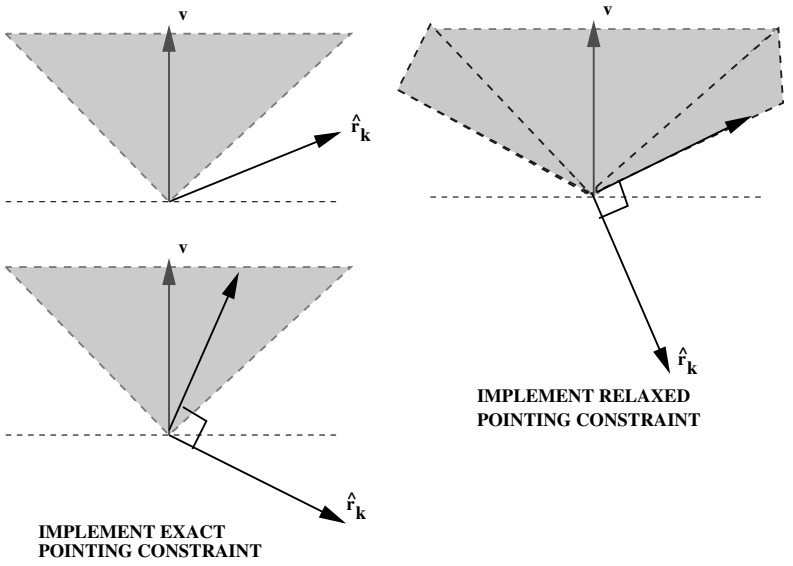

Fig. 9 Graphical interpretation of the thrust pointing constraints.

and $\kappa_{2,k} \geq \gamma$. Then, let $\xi = [v - (v^T \hat{r}_k)\hat{r}_k]/\kappa_{2,k}$. This implies that $\xi^T \hat{r}_k = \hat{r}_k^T v(1 - \|\hat{r}_k\|^2)/\kappa_{2,k} = 0$ and $\xi^T v = [1 - (v^T r_k)^2]/\kappa_{2,k}$. Noting that $\kappa_{2,k}^2 = 1 - (v^T r_k)^2$, we obtain $\xi^T \hat{r}_k = \kappa_{2,k} \geq \gamma$, that is, $\xi \in D_k$. So, $\kappa_{1,k} \geq 0$ or $\kappa_{2,k} \geq \gamma$ guarantees that D_k is a nonempty set. If both of these conditions fail to exist, then we relax the thrust pointing constraint by using the inequality (62). In this case $\cos^{-1}(\kappa_{2,k}) > \theta$, and it is known that (which can be proven by following similar steps) the set $\tilde{D}_k = \{\xi\colon \|\xi\| = 1, \hat{r}_k^T \xi \geq 0 \text{ and } v^T \xi \geq \kappa_{2,k}\}$ is nonempty. This implies that an optimal solution of Problem 2 can satisfy the relaxed thrust pointing constraint (62) without violating the minimum thrust magnitude constraint. See Fig. 9 for a graphical description of the preceding discussion, in which the shaded cone around the vector v shows the θ degree cone defining the feasible thrust direction.

The implementation of this heuristic for the thrust pointing constraint is demonstrated on the example described in Sec. V. Here the initial state of the spacecraft is given by

$$r_0 = \begin{bmatrix} 5000 \\ 0 \\ 0 \end{bmatrix}, \qquad \dot{r}_0 = \begin{bmatrix} 0 \\ 0 \\ 0 \end{bmatrix}$$

that is, the spacecraft is 5000 m above the target landing point. The minimum fuel trajectory for this problem requires that the thrust vector initially points in the opposite direction to the gravity vector, and it later reverses the direction and points in the direction of gravity (see Fig. 10 for simulation results). We repeat the same example with the thrust pointing constraint where

$$v = \begin{bmatrix} 1 \\ 0 \\ 0 \end{bmatrix} \quad \text{and} \quad \gamma = 0$$

that is, the net thrust vector must be in 90 deg cone around the positive x axis. Clearly, when the thrust pointing constraint is not

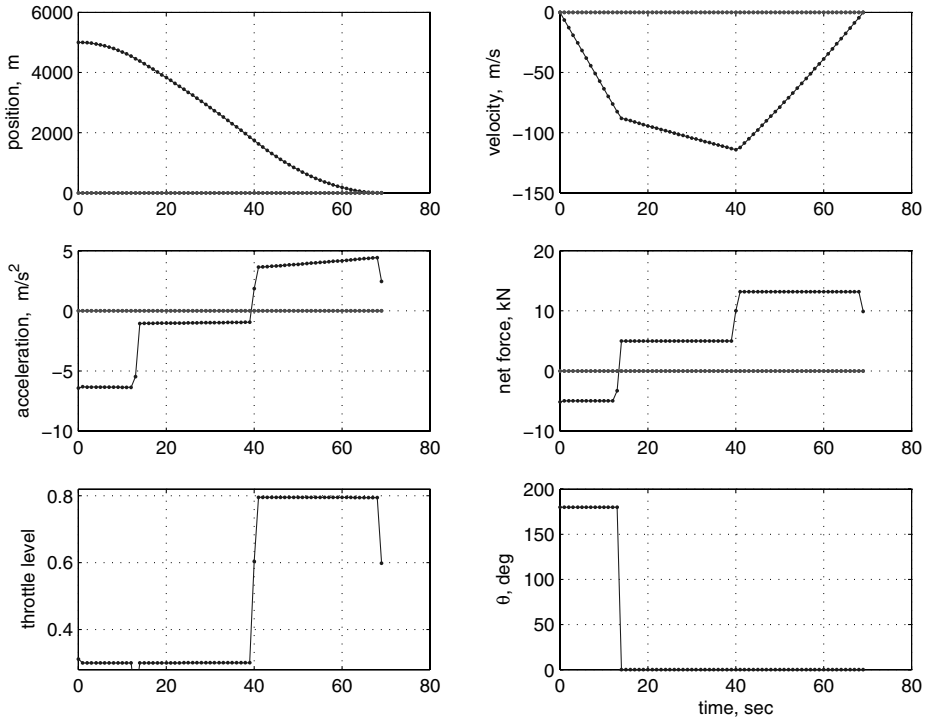

Fig. 10 $r_0 = [5, 0, 0]^T$ km, $\dot{r}_0 = [0, 0, 0]^T$ m/s, $t_f^* = 69$ s, fuel usage = 293.6 kg without thrust pointing constraint.

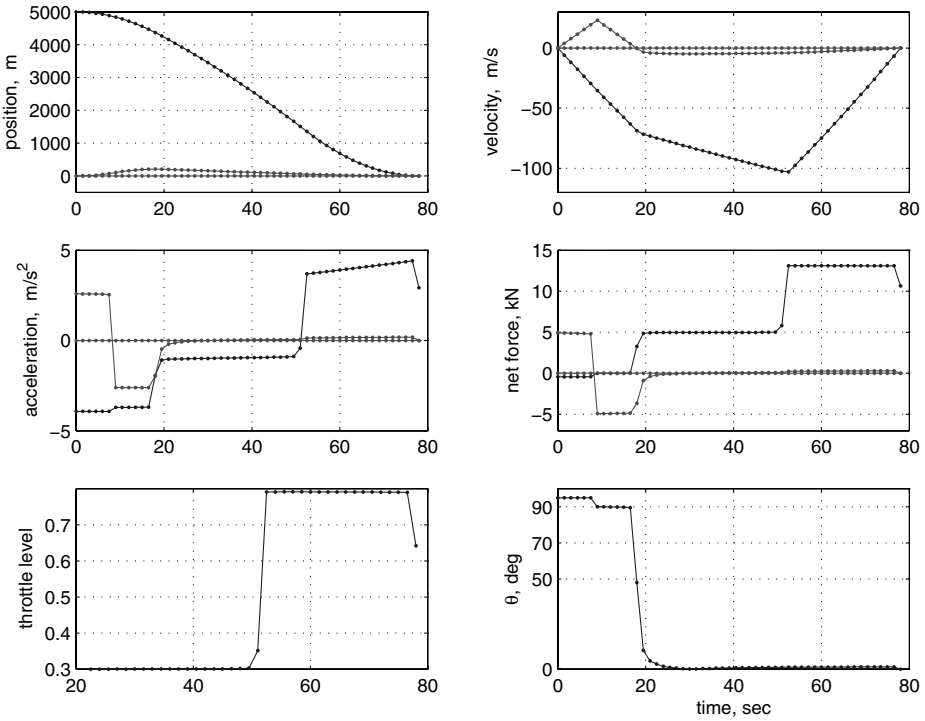

Fig. 11 $r_0 = [5, 0, 0]^T$ km, $\dot{r}_0 = [20, 0, 0]^T$ m/s, $t_f^* = 78$ s, fuel usage = 303 kg with thrust pointing constraint.

enforced, $v^T u(t) < 0$ for the first 14–15 s of the optimal trajectory that violates (61), and the angle of violation is 90 deg. The simulations including the thrust pointing constraint is given in Fig. 11. The thrust pointing constraint is not exactly satisfied for the first 12 s, but it is satisfied afterwards. The violation of the pointing constraint in the first 12 s is due to the relaxation of the pointing constraint described earlier, and the angle of violation is less than 5 deg, which was 90 deg when the constraint (61) was not imposed. Note that, when the pointing constraint was not imposed, the optimal trajectory was a straight line connecting the initial point to the final one, and imposing the pointing constraint lead to a trajectory that is not a straight line. Also, the optimal trajectory with the thrust pointing constraint requires approximately 10 kg more fuel.

VII. Conclusions

In this paper, a powered descent guidance algorithm for Mars pinpoint landing is developed. This algorithm is designed to solve the minimum fuel trajectory optimization problem associated with the pinpoint landing via a direct numerical method. Our main contribution is the formulation of the trajectory optimization problem with nonconvex control constraints as a finite-dimensional convex optimization problem, specifically as a finite-dimensional SOCP (second-order cone program). SOCP problems are a subclass of SDP (semidefinite programming) problems that can be solved in polynomial time with currently available algorithms. The SDP solution algorithms, such as interior-point algorithms, compute a global optimum very efficiently with a deterministic stopping criteria and with prescribed level of accuracy. This is a particularly attractive feature of the numerical solution algorithm because a generic nonlinear programming algorithm cannot in general guarantee a deterministic convergence to a global optimum for a nonlinear optimization problem. Consequently, this guidance algorithm has the *potential* for onboard implementation.

Future work needed for this algorithm can be summarized as follows:

1) We used a generic solver to solve the SOCP problems, and did not make specific effort to implement a SOCP algorithm tailored to solve the Mars pinpoint landing guidance problem. Future work is needed to implement such a SOCP algorithm to improve the speed of the computations, so that the resulting software can be real-time onboard implementable.

2) The constraints due to thrust direction must be further investigated to guarantee their exact satisfaction (or at least quantify the achievable limits of constraint satisfaction).

3) In this paper, we only presented an algorithm to solve the powered descent portion of the Mars pinpoint landing guidance problem. There is a *parachute descent phase* before the powered descent. Specifically, the powered descent phase is initiated by cutting the parachute off. Therefore, the optimal choice of the parachute cutoff time is a critical problem, and we are currently developing algorithms to determine this cutoff time based on the powered descent algorithm presented in this paper. These results will be the subject of a future paper.

4) The explicit consideration of the spacecraft attitude dynamics as a part of the pinpoint landing guidance problem is another future research objective (6-degree-of-freedom guidance problem).

5) A performance comparison study of this guidance algorithm with currently available onboard implementable algorithms will be useful to demonstrate the advantages of this convex approach. Such a study must also include a clear quantification of the computation time needed for the numerical optimization on a realistic onboard computer. This study will potentially make a strong case to use this guidance algorithm onboard a future spacecraft that will land on Mars or the moon.

Acknowledgments

We wish to gratefully acknowledge Aron A. Wolf, Wyatt R. Johnson, Richard Kornfeld, Gurkirpal Singh, Daniel P. Scharf, and David S. Bayard of the Jet Propulsion Laboratory (JPL), and Kenneth D. Mease, Ufuk Topcu, and Federico Najson of University of California, Irvine, for their very valuable comments and suggestions. We also acknowledge Fred Y. Hadaegh of JPL for his encouragements to write this paper. This research was performed at the Jet Propulsion Laboratory, California Institute of Technology, under the contract with National Aeronautics and Space Administration.

References

[1] Wolf, A. A., Graves, C., Powell, R., and Johnson, W., "Systems for Pinpoint Landing at Mars," AAS Paper 04-272, 2004.

[2] Meditch, J. S., "On the Problem of Optimal Thrust Programming For a Lunar Soft Landing," *IEEE Transactions on Automatic Control*,

Vol. AC-9, No. 4, 1964, pp. 477–484.
[3] Flemming,W. H., and Rishel, R. W., *Deterministic and Stochastic Optimal Control*, Springer–Verlag, Berlin, 1975.
[4] Miele, A., *The Calculus of Variations in Applied Aerodynamics and Flight Mechanics in Optimization Techniques*, edited by G. Leitmann, Academic Press, New York, 1962.
[5] Klumpp, A. R., "Apollo Lunar Descent Guidance," *Automatica*, Vol. 10, No. 2, 1974, pp. 133–146.
[6] Topcu, U., Casoliva, J., and Mease, K., "Fuel Efficient Powered Descent Guidance for Mars Landing," AIAA Paper 2005-6286, 2005.
[7] Sostaric, R., and Rea, J., "Powered Descent Guidance Methods for the Moon and Mars," AIAA Paper 2005-6287, 2005.
[8] Najson, F., and Mease, K., "A Computationally Non-Expensive Guidance Algorithm for Fuel Efficient Soft Landing," AIAA Paper 2005-6289, 2005.
[9] Betts, J. T., "Survey of Numerical Methods for Trajectory Optimization," *Journal of Guidance, Control, and Dynamics*, Vol. 21, No. 2, 1998, pp. 193–207.
[10] Hull, D. G., "Conversion of Optimal Control Problems into Parameter Optimization Problems," *Journal of Guidance, Control, and Dynamics*, Vol. 20, No. 1, 1997, pp. 57–60.
[11] Fahroo, F., and Ross, I. M., "Direct Trajectory Optimization by a Chebyshev Pseudospectral Method," *Journal of Guidance, Control, and Dynamics*, Vol. 25, No. 1, 2002, pp. 160–166.
[12] Vlassenbroeck, J., and Dooren, R. V., "A Chebyshev Technique for Solving Nonlinear Optimal Control Problems," *IEEE Transactions on Automatic Control*, Vol. 33, No. 4, 1988, pp. 333–340.
[13] Berkovitz, L. D., *Convexity and Optimization in* $\mathbb{R}^n$, Wiley, New York, 2002.
[14] Boyd, S., and Vandenberghe, L., *Convex Optimization*, Cambridge Univ. Press, Cambridge, England, 2004.
[15] Vandenberghe, L., and Boyd, S., "Semidefinite Programming," *SIAM Review*, Vol. 38, No. 1, 1995, pp. 49–95.
[16] Nesterov, Y., and Nemirovsky, A., *Interior-Point Polynomial Methods in Convex Programming*, SIAM, Philadelphia, PA, 1994.
[17] Sturm, J. F., "Using SeDuMi 1.02, a MATLAB Toolbox for Optimization Over Symmetric Cones," *Optimization Methods and Software*, Vol. 11, No. 1, 1999, pp. 625–653.
[18] Ye, Y., *Interior Point Algorithms*, John Wiley & Sons, New York, 1997.
[19] Sturm, J. F., "Implementation of Interior Point Methods for Mixed Semidefinite and Second Order Cone Optimization Problems," *Optimization Methods and Software*, Vol. 17, No. 6, 2002, pp. 1105–1154.
[20] Ploen, S., Acikmese, B., and Wolf, A., "A Comparison of Powered Descent Guidance Laws for Mars Pinpoint Landing," AIAA Paper 2006-6676, 2006.
[21] Kim, Y., and Mesbahi, M., "Quadratically Constrained Attitude Control via Semidefinite Programming," *IEEE Transactions on Automatic Control*, Vol. 49, No. 5, 2004, pp. 731–735.
[22] Kim, Y., Mesbahi, M., Singh, G., and Hadaegh, F. Y., "On the Constrained Attitude Control Problem," AIAA Paper 2004-5129, Aug. 2004.
[23] Berkovitz, L. D., *Optimal Control Theory*, Springer–Verlag, Berlin, 1975.
[24] Macki, J., and Strauss, A., *Introduction to Optimal Control Theory*, Springer–Verlag, Berlin, 1982.
[25] Bartle, R. G., *The Elements of Integration and Lebesgue Measure*, John Wiley & Sons, Berlin, 1985.
[26] Rudin, W., *Principles of Mathematical Analysis*, 3rd ed., McGraw–Hill, New York, 1976.
[27] Acikmese, B., and Ploen, S., "A Powered Descent Guidance Algorithm for Mars Pinpoint Landing," AIAA Paper 2005-6288, 2005.
[28] Bertsekas, D. P., *Nonlinear Programming*, 2nd ed., Athena Scientific, Belmont, MA, 2000.